Alkaline Metal Reagent-Assisted Synthesis of Monodisperse Iron Oxide Nanostructures

Kwan Lee [1] [iD], Sangyeob Lee [2], Min Chul Oh [1] and Byungmin Ahn [1,3,*] [iD]

[1] Department of Energy Systems Research, Ajou University, Suwon 16499, Korea; kwan308@gmail.com (K.L.); minlovehyo@ajou.ac.kr (M.C.O.)
[2] Wuhan China Star Optoelectronics Technology Co., Ltd., Wuhan 430078, China; sangyeob@gmail.com
[3] Department of Materials Science and Engineering, Ajou University, Suwon 16499, Korea
[*] Correspondence: byungmin@ajou.ac.kr; Tel.: +82-31-219-3531

Abstract: The solvothermal decomposition of iron complexes using the heat-up process enables monodisperse Fe_3O_4 nanoparticle synthesis. Here, we demonstrate that the high reduction potential capability of alkaline metal reagents in the reductive environment allows for pure magnetite phase formation at 200 °C, which is lower than that of typical synthetic method and offers highly crystalline superparamagnetic and ferrimagnetic nanostructures with the ability to control uniformity including spherical and cubic morphology with narrow size distributions. Our method involved reduction of the acetylacetonate and acetate anions to aldehyde and alcohol as an oxygen resource for iron oxide nucleation in an inert condition. For confirming the developed pure surface phase of alkaline metal reagent-assisted magnetite nanoparticle, the magnetic field-dependent shifting of blocking temperature was investigated. The degree of the exchange interaction between core spins and disordered surface spins is attributed to the ratio of core spins and disordered surface spins. The decrease in disordered surface spins deviation due to an enhanced pure phase of magnetite nanoparticles exhibited the negligible shift of the blocking temperature under differently applied external field, and it demonstrated that alkaline metal reagent-induced reductive conditions enable less formation of both disordered surface spins and biphasic nanostructures.

Keywords: alkaline metals; iron oxide; magnetic nanoparticles; superparamagnetic; blocking temperatures; surface disordered spins; surface anisotropy

1. Introduction

Monodisperse magnetic nanostructures have attracted significant interest over last decade due to their importance for both fundamental science and technological applications [1–4]. Their unique magnetic properties allow for ferrofluids, data recording, and medical applications in drug delivery, magnetic resonance imaging (MRI) and hyperthermal cancer treatment [5–7]. Among advanced approaches for magnetic nanocrystal synthesis including co-precipitation reactions [8,9], sol-gel [10], hydrothermal/solvothermal [11], and microemulsion or microwave-assisted methods [12], the formation of monodisperse Fe_3O_4 nanoparticles has been demonstrated with two typical wet chemical synthetic approaches: (I) solvothermal decomposition of iron (III) oleate complexes; and (2) reductively enhanced reaction using iron (III) acetylacetonate reagents with oleylamine under the reflux condition of high-temperature organic solvents [13–15]. While abundant chemical synthetic routes have been reported to obtain uniform magnetic nanostructures with size, shape and chemical composition control, however, the tailoring of enhanced pure phase over various iron oxide polymorphology remains a synthetic challenge without the constraint of size due to unstable nanoscale surface and interface which involved phase transformation resulting in unwanted core-shell nanostructures [13,16,17]. Here, we report a well-defined

dimensional and phase-controlled synthetic method for magnetite nanostructures, assisted by alkaline metal precursors that show higher reduction potentials than that of iron complexes reagent.

Fe_3O_4 nanoparticle is a common magnetic iron oxide nanostructure with an inverse spinel cubic structure in which oxygen forms a face-centered cubic (FCC) closed packing, and Fe cations occupy interstitial tetrahedral sites and octahedral sites [16]. In the case of organic phase synthesis, the high-temperature thermal decomposition of iron (III) oleate complexes in alkene hydrocarbon solvent (e.g., 1-octadecene) is a versatile method for monodisperse magnetite nanoparticles [13]. The decomposition to iron (II) oleate intermediate continuously happened during the heating-up stage and the complete decomposition of iron oleate complexes was allowed at reflux temperature under an inert environment [18]. It readily nucleates wüstite (FeO) phase due to reduction effect of alkene hydrocarbon solvent and the synthesized iron oxide nanoparticles can be oxidized to magnetite after exposure in the air [13]. In contrast, the reductive environment using oleylamine with aromatic ether (e.g., dibenzyl ether) has been applied for the uniform nucleate and growth of iron oxide nanoparticles [14]. An excess amount of oleylamine gave a strong reductive environment and brought the decomposition temperature down to 170 °C. The nucleation of spinel-structured iron oxide nanostructures was directly produced rather than forming intermediate phase (e.g., FeO) first; because the modulated reductive environment with oleylamine led to the reduction of iron cations as well as anion reagent [19]. For instance, the acetylacetonate and acetate anions can be reduced to aldehyde and alcohol as an oxygen resource for iron oxides nucleation in an inert condition [20–22]. In this context, the magnetite phase nanoparticles with the enhanced reductive condition were readily produced at 200 °C [14].

Although the typical approaches using both iron oleate in 1-octadecne and iron (III) acetylacetonate in oleylamine/benzyl ether are resourceful for forming uniform iron oxide nanoparticles, the monodisperse size distribution of magnetite nanoparticles showed the size control limitation (e.g., less than 10 nm in the diameter with oleylamine/benzyl ether) [13,14]. To increase the size of magnetite nanoparticles, the synthesis using iron (III) oleate precursors frequently obtains biphasic nanostructures consisting of a wüstite (antiferromagnetic (AFM) below Neel temperature) core and a spinel (ferrimagnetic (FiM)) shell at which the overall magnetization significantly lowers compared to single-phase Fe_3O_4 nanoparticles [13,18]. The weakness of the oleate-based approach was improved via applying partial oxygen condition and post-treatment using magnetic field-stimulated phase transformation in ambient conditions [16,18,23]. However, purging of oxygen within the as-prepared crude solution enables the formation of a maghemite (γ-Fe_2O_3) phase even at 200 °C [24]. In addition, the reductive effect of oleylamine on iron (III) acetylacetonate is critical for obtaining a uniform nucleation and the redox activity of aromatic ether solvents at reflux temperature enables generation of intermediated radical products including aldehyde group for potential oxidative agents [16]. The harsh conditions with refluxed aromatic ether solution resulted in excess oxidation on the synthesized nanostructures, which formed maghemite phase surface depending on the reaction time [24]. In this context, it is critical to control the reductive nature of iron (III) complex in the decomposition reaction method. Furthermore, it is crucial for reducing to iron (II) complex to form unstable wüstite as nuclei that were readily oxidized into magnetite phase at 200 °C to avoid the formation of maghemite phase. We found that an alkaline metal acetate reagent involving high reduction potential (e.g., magnesium acetate) lead to the burst nucleation of magnetite nanoparticles in the organic solvent phase around 180–200 °C at which an oxygen source can be generated from decomposed acetylacetonate and acetate anions which are working as an oxidizing agent. The addition of alkaline metal acetate reagents opens up the lower temperature synthesis of superparamagnetic magnetite nanocrystals without reflux temperature condition, which can cause phase mixture with maghemite phase. Furthermore, the usage of alkaline metal precursor enables a low-cost synthetic process without a high-cost reducing agent (e.g., 1,2-Hexadecanediol (HDD)).

2. Materials and Methods

2.1. Iron Oxide Nanoparticles Synthesis

Magnetite nanoparticles were prepared using alkaline metal precursors (magnesium acetate tetrahydrate (Sigma-Aldrich, >99.9%, St. Louis, MO, USA)) and iron (III) acetylacetonate (Sigma-Aldrich, >99.9%) added in the mixture of oleylamine (Sigma-Aldrich, 70%, St. Louis, MO, USA), benzyl ether (Aldrich, 90%, St. Louis, MO, USA) in a three-neck flask and magnetically stirred at room temperature. The concentration of alkaline metal agents kept the ratio of Mg/Fe in the range from 0.1 to 0.3. The higher concentration of alkaline metal reagent (e.g., over 0.3) produced the amorphous phase formation at the 200 °C and the maghemite phase with alkaline metal doping was obtained under a reflux temperature condition. 3 mmol of iron (III) acetylacetonate was kept in this study. The size of the magnetic nanoparticles was controlled by the different quantity of oleylamine. In a typical synthesis of 18 nm Fe_3O_4 nanoparticles, the volume ratio of oleylamine to benzyl ether was 15 mL/15 mL and higher ratio provided the smaller size of ferrite nanoparticles. The mixture solution was heated up to 200 °C for 30 min and it maintained for another 60 min. After the heat treatment process, the resultant solution was cooled down to room temperature and ethanol/toluene mixture was added. The synthesized nanoparticles were collected by centrifugation and the obtained product was washed several times and stocked with polar solvents.

2.2. Iron Oxide Nanocubes Synthesis

The mixture of iron (III) acetylacetonate (3 mmol), magnesium acetate, oleic acid and sodium oleate was placed in a three-neck round bottom flask containing 15 mL/15 mL of oleylamine/benzyl ether. The reaction mixture was heated up to 120 °C for 30 min to dissolve all solids and kept for additional 30 min. The reduction and nucleation allowed for the black color of reaction temperature of 200 °C for 30 min with vigorous stirring. The same condition alkaline metal reagent for spherical morphology was identically applied to nanocubes formation. The size of nanocubes was controlled by different sodium oleate from 1 mmol to 3 mmol. The result nanocubes were precipitated with the addition of a mixture of hexane/ethanol and the clear supernatant was discarded. The precipitated solids were redispersed in *n*-hexane.

2.3. Structural and Compositional Characterization

The average particle size and shape of as-synthesized nanoparticles was examined using a field-emission transmission electron microscopy (JEOL 2100F FE-TEM, Tokyo, Japan) and energy dispersive spectrometer to confirm chemical composition and existence of alkaline metal ions residue within the synthesized nanoparticles. X-ray diffraction (XRD, Bruker D8 Advance X-ray diffractometer, Karlsruhe, Germany) was employed for crystalline structure analysis of synthesized magnetite nanoparticles. X-ray photoelectron spectroscopy (XPS, Scienta-Gammadata ESCA 200, Uppsala, Sweden) measurements equipped with a monochromatized Al Kα. X-ray source (1486.6 eV) was carried out. The synthesized colloidal solutions in stock solution were deposited on a silicon substrate, inserted in the load lock chamber and then dried in vacuum before the XPS analysis. All samples were charge compensated by an electron gun. Wide scans were acquired in the binding energy (BE) range 20–1200 eV for all the samples.

2.4. Magnetic Properties

The blocking temperature of superparamagnetic magnetite nanoparticles (8.5 mg in the range of temperature from 50 K to 150 K with the applied magnetic field (50 Oe)) was determined by the ZFC (Zero Field Cooling)-FC (Field Cooling) measurement. A superconducting quantum interference device (Quantum Design MPMS 3 SQUID Magnetometer, San Diego, CA, USA) with simple correction method for the sample shape and radially offset effects were used. Magnetic hysteresis loops of all nanoparticles

were measured under the maximum magnetic field of ±15,000 Oe (1.5 Tesla) at room temperature with Vibrating Sample Magnetometer (VSM, Lake Shore Model 7404, Westerville, OH, USA).

3. Results and Discussion

The schematic of our synthetic method shown in Figure 1a outlines the alkaline metal acetate reagent-assisted magnetite nanoparticles synthesis as representatives with magnesium acetate. The decomposed acetylacetonate and acetate anions can enable reduction to aldehyde and alcohol as oxygen resource with a high reduction potential of alkaline metal ions in the reductive environment. For alkaline metal reagent-assisted magnetite nanoparticles formation, we choose magnesium acetate based on the following considerations: (1) alkaline metal reagent can be decomposed at a lower temperature than that of iron (III) reagent; (2) species with relatively small ionization energies is preferred; and (3) higher reducing potential than that of iron reagent is crucial to avoid precipitation of alkaline metal oxide or alloy [25,26].
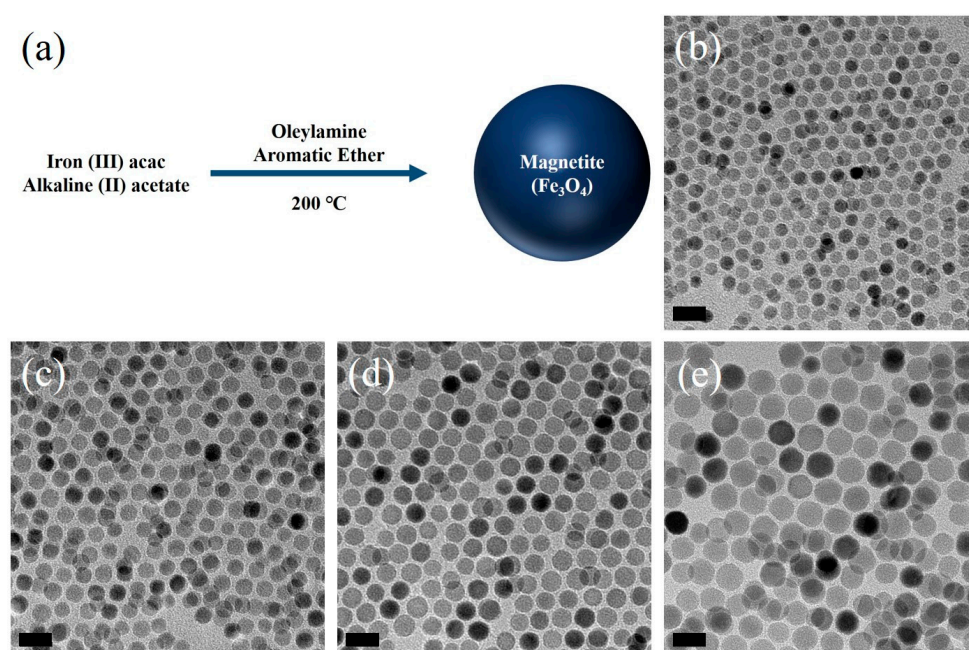

Figure 1. Spherical magnetic nanoparticles with the alkaline metal reagent. (**a**) Schematic formation path of spherical magnetite nanoparticles assisted by alkaline metal complexes. TEM images of monodisperse magnetite nanoparticles with sizes of (**b**) 8 nm, (**c**) 11 nm, (**d**) 15 nm, and (**e**) 18 nm with the different volume ratio of oleylamine/ether. Scale bar is 20 nm.

The color transition from red to brown happened after decomposition of $Fe(acac)_3$ and then the reduction and nucleation led to the black color at the reaction temperature (200 °C) with time. The oleylamine can act as surfactant of weaker ligand during the reaction for giving spherical Fe_3O_4 nuclei due to negligible energy difference for different crystal planes on the surface of the nuclei [27]. It is worth noting that amorphous iron oxide phase nuclei at the initial stage reaching 200 °C were readily oxidized to magnetite phase which was confirmed with powder X-ray diffraction method (Figure S1). Under the identical conditions to previous reports, our amorphous phase nucleation can readily lead to the formation of larger nucleation which allows for the larger size of magnetite nanoparticles that that of the previous reports without the alkaline metal reagents [10]. The crystallization at 200 °C for 1 h reaction time allowed for the formation of magnetite phase with homogeneous spherical shape. The higher temperature than 200 °C can enable improvement of magnetite phase formation; however, XPS analysis showed that fully oxidized maghemite phase transformed from magnetite can exist over 200 °C (Figure S2). Furthermore, the size of magnetite

nanoparticles was controlled with a volume ratio of oleylamine and aromatic ether. Uniform magnetite nanoparticles with tailoring size from 8 nm to 18 nm were confirmed by transmission electron microscopy (TEM) as shown in Figure 1b–e. The 18 nm magnetite nanoparticles were obtained from the condition using a mixture of oleylamine (15 mL) and ether (15 mL). The smallest size (8 nm) of the nanoparticles in this study was obtained when only oleylamine was used. Compared with the previous report [14], our approach with alkaline metal reagents provided an increase in the size under the identical condition of the oleylamine/aromatic ether ratio. We washed out the unreacted and residue of alkaline metal reagent with toluene/ethanol mixture, which was confirmed by energy dispersive analysis and thermogravimetric analysis (TGA) (Figures S3 and S4).

We performed the magnetic studies of major (15,000 Oe) and minor (150 Oe) magnetization (M)-field (H) characteristics using a vibrating sample mode magnetometer (VSM, Quantum Design PPMS, San Diego, CA, USA) at room temperature as shown in Figure 2a. Spherical iron oxide nanoparticles with different size from 8 nm to 18 nm show the typical characteristics of superparamagnetic behavior with saturation magnetization values (up to 75 emu/g at 18 nm) smaller than the bulk magnetite (92 emu/g) at room temperature. The saturation magnetization decrease agreed with the presence of the surface spin effect enhancement while the size of magnetite nanoparticles reduced. Furthermore, the coercivity and remanence magnetization value from the minor hysteresis curves with 150 Oe maximum field in the inset of Figure 2a shows very close to zero. We also confirmed that the degree of magnetization increment in minor hysteresis curves was attributed to a surface spin effect. The magnetization versus temperature measurement was performed in zero-field cooling (ZFC) with a 50 Oe probe field in Figure 2b. Convergence of ZFC-FC mode curves above the blocking temperature was observed, which is coincident with an irreversible temperature of superparamagnetism (Figure S5). The normalized magnetization-dependent temperature exhibited the maximum peak shift of ZFC mode curve to higher temperature with the increase of the nanoparticles sizes. We observed the blocking temperature to be 78 K for 18 nm magnetite nanoparticles, which decrease to 58 K for the 8 nm magnetite nanoparticles due to an enhancement in magnetocrystalline anisotropy energy for the larger particles sizes [28].
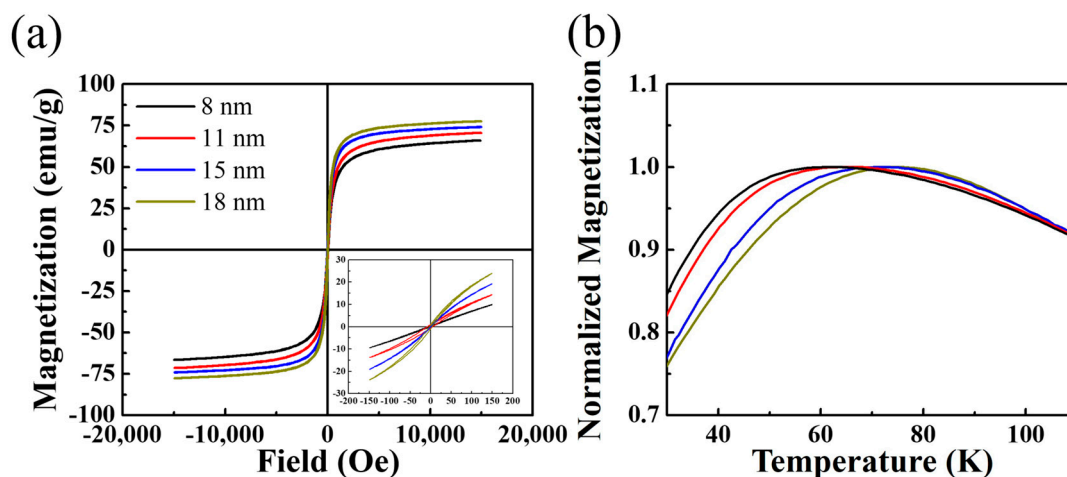

Figure 2. Magnetic properties of iron oxide nanoparticles synthesized with alkaline metal reagent (**a**) Superimposed room temperature field-dependent magnetization loop of different sizes of magnetite nanoparticles. The inset in (**a**) shows minor M-H hysteresis curve; (**b**) Temperature-dependent normalized magnetization plot under 50 Oe for magnetite nanoparticles of different size under zero-field cooling (ZFC) magnetization.

The magnetic field-dependent exchange interaction between core spins and disordered surface spins within corresponding nanostructures was reported by the field-dependent shift of blocking temperature [29]. The alignment of disordered surface spins is dependent on the strength of the

external magnetic field, at which the exchange coupling led to the variation of extrinsic blocking temperature as maximum point of ZFC characteristics, and their interaction was not associated with the dipole-dipole interaction. In this context, higher exchange coupling led to higher extrinsic blocking temperature due to the contribution of disordered surface spins.

We synthesized two magnetite nanoparticles with identical size (15 nm) and spherical morphology. One ($MNP_{alkaline}$) was obtained using alkaline metal reagent at 200 °C, and the other ($MNP_{typical}$) was produced without alkaline metal reagents at reflux temperature conditions of organic solvent. To evaluate a blocking temperature under the different external magnetic field, we performed a ZFC mode measurement using Superconducting Quantum Interference Devices (SQUIDs) under differently applied magnetic field (15 Oe, 30 Oe, and 50 Oe) from 50 K to 150 K in Figure 3. At the condition of the lowest field of 15 Oe showed in Figure 3a in this study, the $MNP_{alkaline}$ (open square in Figure 3) showed lower blocking temperature with higher magnetization value than that of the $MNP_{typical}$ (solid square in Figure 3). A high degree of exchange interactions between the core spins and disordered surface spins under 15 Oe magnetic field result in higher blocking temperature of ~88 K for $MNP_{typical}$ comparing with ~73 K for $MNP_{alkaline}$. We understood that the alkaline metal reagent-assisted magnetite nanoparticles were less affected by surface disordered spins on exchange coupling leading to the negligible change of blocking temperature, which can indirectly present that surface phase was improved with addition of alkaline metal reagents when synthesized. As the blocking temperature is more critical to the nature of the disordered surface spins, the alkaline metal reagent-assisted iron oxide nanoparticles allow for fewer exchange interactions, and the surface spin deviation degree was tailored by treatment of reductive synthetic conditions with alkaline metal complexes. As the external magnetic field increases up to 50 Oe shown in Figure 3b,c, $MNP_{typical}$ showed the variation of extrinsic blocking temperature shifting to the lower temperature from 88 K to 73 K. In contrast, the maximum point of ZFC curves of $MNP_{alkaline}$ shows the negligible change of the extrinsic blocking temperature (~73 K). Under the magnetic field with 50 Oe, both magnetic nanoparticles of $MNP_{alkaline}$ and $MNP_{typical}$ showed identical blocking temperatures and magnetization. Enhanced magnetic phase enables less disordered surface spins effect in magnetic nanoparticles and it was understood overall spin deviation regarding external magnetic field are prevalent at the surface of the spherical nanoparticles [30]. While a surface topology with low energy surface facet (e.g., (100)) allow for reduced surface anisotropy comparing between the spherical and cubic morphology of magnetic nanoparticles, however, a surface phase during the synthetic treatment can lead to different surface anisotropy from our investigation. Our synthetic method enabled the decrease in disordered surface spins degree with stable magnetite phase assisted by the alkaline metal reagent at the point of field-dependent exchange interaction effect.
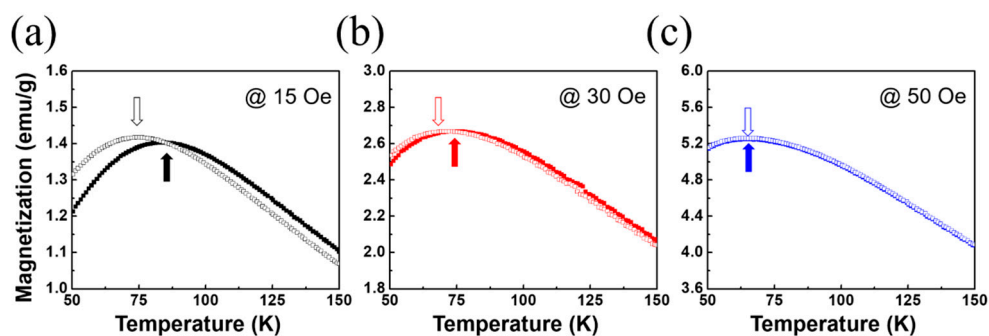

Figure 3. A blocking temperature shift effect depending on an external magnetic field under ZFC condition. The blocking temperature of two 15 nm magnetite nanoparticles synthesized with (open square) and without (solid square) alkaline metal complexes was compared with internal exchange coupling between core spins and disordered surface spins (**a**) under the external magnetic field of 15 Oe; (**b**) For an increase of the external magnetic field, exchange coupling leads to blocking temperature shifted to lower value; (**c**) all core spins were aligned to the magnetic field and the difference of exchange coupling effect was negligible under the magnetic field of 50 Oe.

Compared with spherical iron oxide nanostructures, the iron oxide nanocubes present superior magnetic properties and enhanced hyperthermia performance for a cancer treatment due to their higher magnetic anisotropic characters [31]. Furthermore, directionality and packing behavior made cubic nanoparticles of significant interest for the study of self-assembled nanostructures [32]. In a typical synthesis, fast heat-up process (heating rate of over 15 °C/min) of a mixture of Fe(acac)$_3$, oleic acid, and aromatic ethers was reported to offer the ability of size control in the range from 22 nm to 160 nm for ferromagnetic nanocubes [33]. However, the heat-up condition is critical to control uniform size, shape, but it is challenging to apply to the mass production process. In addition, thermal decomposition of iron (III) oleate with a mixture of sodium oleate and alkane hydrocarbon solvent demonstrated the cubic morphology under the reflux condition of high boiling temperature organic phase for superparamagnetic nanocubes [32]. The oleate precursor approach limits the size of the superparamagnetic regime and showed polyphase core-shell structures in the regime of ferromagnetic nanostructures respectively.

In this context, our new approach with unique advantages of mild conditions (lower process temperature than reflux condition, mild heating rate, less usage of organic surfactant) can further provide a tantalizing opportunity to obtain the well-defined magnetite nanocubes with size control. Our facile strategies with alkaline metals reagents enable the solvothermal decomposition of iron precursors with sodium oleate around 200 °C for the formation of the monodisperse magnetite nanocubes as shown in Figure 4 and Figures S6–S8. Figure 4a schematically outlines the process of an alkaline metal-assisted synthetic method for uniform magnetic nanocubes. In this synthetic route, the alkaline metal reagent was decomposed and anion complex from alkaline reagents working as the oxidation agent which is an identical reaction mechanism for spherical nanoparticles synthesis shown in Figure 1. Sodium oleate as surfactant has a high binding affinity to a specific crystalline facet and regulates the competitive growth in the <100> direction over the <111> direction with crystalline facet (100) of inverse spinel cubic structures which is leading to the fast growth along <111> direction and the final nanocubes surfaces are corresponding to (100) plane. The TEM image shown in Figure 4b–d revealed that the dimensions of the nanocubes could be controlled by varying the experimental conditions of sodium oleate concentration. Our versatile method provides uniform edge length of 22 ± 1.2 nm, 36 ± 2.5 nm, 57 ± 5.1 nm by controlling the quantity of sodium oleate, which is described in materials and method section. The high-resolution TEM (HRTEM) image in Figure 4e shows the highly crystalline feature of the nanocubes with the measured d-spacing value (2.10 Å) of (400) magnetite plane.
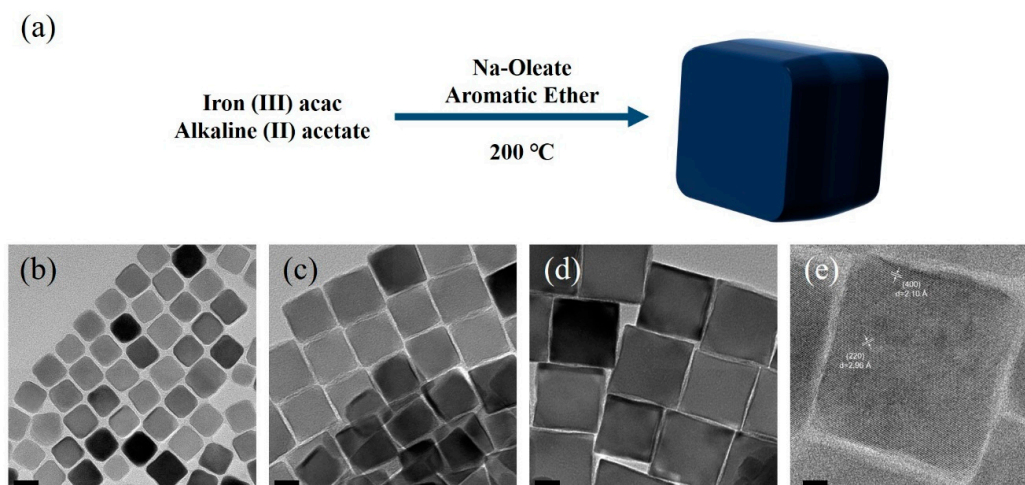

Figure 4. Scheme of Iron oxide nanocubes synthesis and TEM characterization. (**a**) Schematic of a synthetic method for magnetite nanocubes; (**b**–**d**) large area transmission electron microscopy (TEM) images of monodisperse magnetite nanocubes with alkaline metal ions assistance with the size distribution of 22 ± 1.2 nm, 36 ± 2.5 nm, 57 ± 5.1 nm in edge length with less 10% deviation. Scale bar is 20 nm (**d**) high-resolution TEM image for structural characterization. Scale bar is 5 nm.

4. Conclusions

In conclusion, we demonstrated a facile method to synthesize enhanced pure phase and monodisperse magnetite nanoparticles and nanocubes. The alkaline metal reagents enable a lower reaction temperature than typical protocols using reflux conditions of an organic solvent. High reduction potential capability allows for the generation of intermediate oxidizing species from anions reagents, which produced a larger size than that of the reductively enhanced synthetic method without alkaline metal complexes. A burst reduction of iron reagents enables less usage of both capping agent and reducing agent and burst nucleation of monodisperse nanocrystals at low temperature. Our alkaline metal-assisted synthetic method for magnetite nanostructure allows for the enhanced pure phase of magnetite nanoparticles, and the blocking temperature variation due to exchange interplay between core spins and disordered surface spins depending on the external magnetic field indirectly elucidated by the state of the less-disordered surface spins. The shifting of blocking temperature represented the existence of disordered surface spins of magnetic nanoparticles, and we demonstrate the undetectable shifting of blocking temperature is associated with improved surface phase-assisted alkaline metal species during the nanoparticle formation.

Supplementary Materials: The following are available online at http://www.mdpi.com/2075-4701/8/2/107/s1, Figure S1: XRD measurement confirmed the crystalline structure of magnetite nanoparticles with two samples from initial stage (red line, 200 °C, 0 min) and final state (black line, 200 °C, 60 min) of the reaction; Figure S2: The oxidation state of iron at the outer surfaces of the synthesized nanoparticles was further investigated by XPS. While the complex structure of nanoscale samples prevents us from performing a full quantitative deconvolution of the Fe 2p spectra, the main Fe 2p peaks (black arrows) with the characteristic peak profile are observed for two samples which was heated at 200 °C and 250 °C respectively and indicates that the surface of the NPs is predominantly Fe^{3+}. A satellite feature at 718.5 eV (blue arrow) is clearly observed for 250 °C heating condition and this satellite is most pronounced for pure Fe_2O_3 and is not observed for pure Fe_3O_4; Figure S3: Energy Dispersive Spectroscopy (EDS) analysis of synthesized magnetite nanoparticles which was cleaned with a mixture of toluene/ethanol several times. No alkaline metal element was detected; Figure S4: TGA of Fe_3O_4 nanoparticles synthesized with assistance of alkaline metal reagents; Figure S5: ZFC-FC measurement of different size of magnetite nanoparticles; Figure S6: Low magnification TEM images of magnetite nanocubes assisted by alkaline metal ions reductions. Various reagent concentration and reaction time enable the size control of magnetite nanocubes with the size distribution of (a) 22 ± 1.2 nm, (b) 36 ± 2.5 nm, and (c) 57 ± 5.1 nm in edge length. Scare bar is 50 nm; Figure S7: XRD measurement of Fe_3O_4 nanocubes confirmed as inverse spinel cubic structures; Figure S8: Energy Dispersive Spectroscopy (EDS) analysis of synthesized magnetite nanocubes.

Author Contributions: K.L. performed all materials synthesis, and some of characterizations and measurements. S.L. M.C.O. contributed to sample characterizations. K.L. and B.A. formulated the idea and wrote the manuscript. All co-authors participated in discussion and manuscript writing.

Conflicts of Interest: The authors declare no conflict of interest.

References

1. Sun, S.; Murray, C.B.; Weller, D.; Folks, L.; Moser, A. Monodisperse FePt Nanoparticles and Ferromagnetic FePt Nanocrystal Superlattices. *Science* **2000**, *287*, 1989–1992. [CrossRef] [PubMed]

2. Ho, D.; Sun, X.; Sun, S. Monodisperse Magnetic Nanoparticles for Theranostic Applications. *Acc. Chem. Res.* **2011**, *44*, 875–882. [CrossRef] [PubMed]

3. Sun, S.; Zeng, H.; Robinson, D.B.; Raoux, S.; Rice, P.M.; Wang, S.X.; Li, G. Monodisperse MFe_2O_4 (M = Fe, Co, Mn) Nanoparticles. *J. Am. Chem. Soc.* **2004**, *126*, 273–279. [CrossRef] [PubMed]

4. Park, J.; Joo, J.; Kwon, S.G.; Jang, Y.; Hyeon, T. Synthesis of Monodisperse Spherical Nanocrystals. *Angew. Chem. Int. Ed.* **2007**, *46*, 4630–4660. [CrossRef] [PubMed]

5. Wu, L.; Jubert, P.-O.; Berman, D.; Imaino, W.; Nelson, A.; Zhu, H.; Zhang, S.; Sun, S. Monolayer Assembly of Ferrimagnetic $Co_xFe_{3-x}O_4$ Nanocubes for Magnetic Recording. *Nano Lett.* **2014**, *14*, 3395–3399. [CrossRef] [PubMed]

6. Na, H.B.; Song, I.C.; Hyeon, T. Inorganic Nanoparticles for MRI Contrast Agents. *Adv. Mater.* **2009**, *21*, 2133–2148. [CrossRef]

7. Bae, S.; Jeoung, J.W.; Jeun, M.; Jang, J.; Park, J.H.; Kim, Y.J.; Lee, K.; Kim, M.; Lee, J.; Hwang, H.M.; et al. Magnetically Softened Iron Oxide (MSIO) Nanofluid and Its Application to Thermally-Induced Heat Shock Proteins for Ocular Neuroprotection. *Biomaterials* **2016**, *101*, 165–175. [CrossRef] [PubMed]

8. Xia, T.; Wang, J.; Wu, C.; Meng, F.; Shi, Z.; Lian, J.; Feng, J.; Meng, J. Novel Complex-Coprecipitation Route to Form High Quality Triethanolamine-Coated Fe$_3$O$_4$ Nanocrystals: Their High Saturation Magnetizations and Excellent Water Treatment Properties. *CrystEngComm* **2012**, *14*, 5741–5744. [CrossRef]

9. Pereira, C.; Pereira, A.M.; Rocha, M.; Freire, C.; Geraldes, C.F.G.C. Architectured Design of Superparamagnetic Fe$_3$O$_4$ Nanoparticles for Application as MRI Contrast Agents: Mastering Size and Magnetism for Enhanced Relaxivity. *J. Mater. Chem. B* **2015**, *3*, 6261–6273. [CrossRef]

10. Mishra, S.; Jeanneau, E.; Rolland, M.; Daniele, S. Structural Isomers of Iron(III) *N*-Methyl Diethanolaminate as Sol–gel Precursors for Iron-Based Oxide Nanomaterials. *RSC Adv.* **2016**, *6*, 1738–1743. [CrossRef]

11. Liang, X.; Wang, X.; Zhuang, J.; Chen, Y.; Wang, D.; Li, Y. Synthesis of Nearly Monodisperse Iron Oxide and Oxyhydroxide Nanocrystals. *Adv. Funct. Mater.* **2006**, *16*, 1805–1813. [CrossRef]

12. Li, X.; Liu, D.; Song, S.; Wang, X.; Ge, X.; Zhang, H. Rhombic Dodecahedral Fe$_3$O$_4$: Ionic Liquid-Modulated and Microwave-Assisted Synthesis and Their Magnetic Properties. *CrystEngComm* **2011**, *13*, 6017–6020. [CrossRef]

13. Park, J.; An, K.; Hwang, Y.; Park, J.-G.; Noh, H.-J.; Kim, J.-Y.; Park, J.-H.; Hwang, N.-M.; Hyeon, T. Ultra-Large-Scale Syntheses of Monodisperse Nanocrystals. *Nat. Mater.* **2004**, *3*, 891–895. [CrossRef] [PubMed]

14. Xu, Z.; Shen, C.; Hou, Y.; Gao, H.; Sun, S. Oleylamine as Both Reducing Agent and Stabilizer in a Facile Synthesis of Magnetite Nanoparticles. *Chem. Mater.* **2009**, *21*, 1778–1780. [CrossRef]

15. Laurent, S.; Forge, D.; Port, M.; Roch, A.; Robic, C.; Vander Elst, L.; Muller, R.N. Magnetic Iron Oxide Nanoparticles: Synthesis, Stabilization, Vectorization, Physicochemical Characterizations, and Biological Applications. *Chem. Rev.* **2008**, *108*, 2064–2110. [CrossRef] [PubMed]

16. Chen, R.; Christiansen, M.G.; Sourakov, A.; Mohr, A.; Matsumoto, Y.; Okada, S.; Jasanoff, A.; Anikeeva, P. High-Performance Ferrite Nanoparticles through Nonaqueous Redox Phase Tuning. *Nano Lett.* **2016**, *16*, 1345–1351. [CrossRef] [PubMed]

17. Wang, C.; Baer, D.R.; Amonette, J.E.; Engelhard, M.H.; Antony, J.; Qiang, Y. Morphology and Electronic Structure of the Oxide Shell on the Surface of Iron Nanoparticles. *J. Am. Chem. Soc.* **2009**, *131*, 8824–8832. [CrossRef] [PubMed]

18. Kemp, S.J.; Ferguson, R.M.; Khandhar, A.P.; Krishnan, K.M. Monodisperse Magnetite Nanoparticles with Nearly Ideal Saturation Magnetization. *RSC Adv.* **2016**, *6*, 77452–77464. [CrossRef]

19. Crouse, C.A.; Barron, A.R. Reagent Control over the Size, Uniformity, and Composition of Co–Fe–O Nanoparticles. *J. Mater. Chem.* **2008**, *18*, 4146–4153. [CrossRef]

20. Li, D.; Arachchige, M.P.; Kulikowski, B.; Lawes, G.; Seda, T.; Brock, S.L. Control of Composition and Size in Discrete Co$_x$Fe$_{2−x}$P Nanoparticles: Consequences for Magnetic Properties. *Chem. Mater.* **2016**, *28*, 3920–3927. [CrossRef]

21. Turek, T.; Trimm, D.L.; Cant, N.W. The Catalytic Hydrogenolysis of Esters to Alcohols. *Catal. Rev.* **1994**, *36*, 645–683. [CrossRef]

22. Seo, W.S.; Shim, J.H.; Oh, S.J.; Lee, E.K.; Hur, N.H.; Park, J.T. Phase- and Size-Controlled Synthesis of Hexagonal and Cubic CoO Nanocrystals. *J. Am. Chem. Soc.* **2005**, *127*, 6188–6189. [CrossRef] [PubMed]

23. Lak, A.; Niculaes, D.; Anyfantis, G.C.; Bertoni, G.; Barthel, M.J.; Marras, S.; Cassani, M.; Nitti, S.; Athanassiou, A.; Giannini, C.; et al. Facile Transformation of FeO/Fe$_3$O$_4$ Core-Shell Nanocubes to Fe$_3$O$_4$ via Magnetic Stimulation. *Sci. Rep.* **2016**, *6*, 33295. [CrossRef] [PubMed]

24. Hai, H.T.; Kura, H.; Takahashi, M.; Ogawa, T. Facile Synthesis of Fe$_3$O$_4$ Nanoparticles by Reduction Phase Transformation from γ-Fe$_2$O$_3$ Nanoparticles in Organic Solvent. *J. Colloid Interface Sci.* **2010**, *341*, 194–199. [CrossRef] [PubMed]

25. Koga, N.; Suzuki, Y.; Tatsuoka, T. Thermal Dehydration of Magnesium Acetate Tetrahydrate: Formation and in Situ Crystallization of Anhydrous Glass. *J. Phys. Chem. B* **2012**, *116*, 14477–14486. [CrossRef] [PubMed]

26. Haynes, W.M. (Ed.) *CRC Handbook of Chemistry and Physics*, 97th ed.; CRC Press: Boca Raton, FL, USA, 2016.

27. Hou, Y.; Xu, Z.; Sun, S. Controlled Synthesis and Chemical Conversions of FeO Nanoparticles. *Angew. Chem. Int. Ed.* **2007**, *46*, 6329–6332. [CrossRef] [PubMed]

28. Mohapatra, J.; Mitra, A.; Bahadur, D.; Aslam, M. Surface Controlled Synthesis of MFe_2O_4 (M = Mn, Fe, Co, Ni and Zn) Nanoparticles and Their Magnetic Characteristics. *CrystEngComm* **2012**, *15*, 524–532. [CrossRef]

29. Lee, K.; Jang, J.; Nakano, H.; Nakagawa, S.; Paek, S.H.; Bae, S. External Magnetic Field Dependent Shift of Superparamagnetic Blocking Temperature Due to Core/Surface Disordered Spin Interactions. *Nanotechnology* **2017**, *28*, 075710. [CrossRef] [PubMed]

30. Noh, S.; Na, W.; Jang, J.; Lee, J.-H.; Lee, E.J.; Moon, S.H.; Lim, Y.; Shin, J.-S.; Cheon, J. Nanoscale Magnetism Control via Surface and Exchange Anisotropy for Optimized Ferrimagnetic Hysteresis. *Nano Lett.* **2012**, *12*, 3716–3721. [CrossRef] [PubMed]

31. Elsayed, W.E.M.; Al-Hazmi, F.S.; Memesh, L.S.; Bronstein, L.M. A Novel Approach for Rapid Green Synthesis of Nearly Mono-Disperse Iron Oxide Magnetic Nanocubes with Remarkable Surface Magnetic Anisotropy Density for Enhancing Hyperthermia Performance. *Colloids Surf. Physicochem. Eng. Asp.* **2017**, *529*, 239–245. [CrossRef]

32. Singh, G.; Chan, H.; Baskin, A.; Gelman, E.; Repnin, N.; Král, P.; Klajn, R. Self-Assembly of Magnetite Nanocubes into Helical Superstructures. *Science* **2014**, *345*, 1149–1153. [CrossRef] [PubMed]

33. Kim, D.; Lee, N.; Park, M.; Kim, B.H.; An, K.; Hyeon, T. Synthesis of Uniform Ferrimagnetic Magnetite Nanocubes. *J. Am. Chem. Soc.* **2009**, *131*, 454–455. [CrossRef] [PubMed]